Chemical Science

ROYAL SOCIETY OF CHEMISTRY

PERSPECTIVE

View Article Online
View Journal | View Issue

Cite this: *Chem. Sci.*, 2024, **15**, 15954

All publication charges for this article have been paid for by the Royal Society of Chemistry

Received 20th June 2024
Accepted 4th September 2024

DOI: 10.1039/d4sc04065a

rsc.li/chemical-science

Key developments in magnesiothermic reduction of silica: insights into reactivity and future prospects†

Maximilian Yan,‡[ab] Sarah Martell,‡[a] Siddharth V. Patwardhan[b] and Mita Dasog*[a]

Porous Si (p-Si) nanomaterials are an exciting class of inexpensive and abundant materials within the field of energy storage. Specifically, p-Si has been explored in battery anodes to improve charge storage capacity, to generate clean fuels through photocatalysis and photoelectrochemical processes, for the stoichiometric conversion of CO_2 to value added chemicals, and as a chemical H_2 storage material. p-Si can be made from synthetic, natural, and waste SiO_2 sources through a facile and inexpensive method called magnesiothermic reduction (MgTR). This yields a material with tunable properties and excellent energy storage capabilities. In order to tune the physical properties that affect performance metrics of p-Si, a deeper understanding of the mechanism of the MgTR and factors affecting it is required. In this perspective, we review the key developments in MgTR and discuss the thermal management strategies used to control the properties of p-Si. Additionally, we explore future research directions and approaches to bridge the gap between laboratory-scale experiments and industrial applications.

Introduction

As climate change intensifies, efforts to decarbonize and reduce global dependence on fossil fuels have gained momentum. With the rising global energy demand, it is crucial to explore and adopt more sustainable energy sources to replace fossil fuels.[1] Renewable sources of energy such as solar and wind are notable sustainable alternatives to fossil fuels; yet, they have issues with intermittency which makes the storage of renewable energy an important area of research. An exciting material in the field of energy harvesting and storage is porous Si (p-Si) nanostructures as it has been explored as a high capacity anode material,[2–14] photocatalyst[15–23] and photoelectrode for solar driven fuel production,[24–27] for stoichiometric conversion of CO_2 to value-added materials,[28–31] and as a chemical H_2 storage material (Fig. 1).[32,33] What makes p-Si unique and valuable for energy storage applications is its sponge-like pore network. This structure provides a high surface area for chemical reactions and adjustable pore sizes, which can be utilized for light trapping in photocatalysis and to accommodate material expansion in Li-ion batteries. These pores can be in the micro-, meso-, or macro-porous size regime, meaning that they have a diameter of <2 nm, 2–50 nm or >50 nm, respectively. Furthermore, physical properties such as the crystallinity, surface area, pore size distribution, pore volume, and particle size and morphology of p-Si are tunable depending on the synthetic route and reaction conditions used.[34] Understanding how to tailor these properties is of significance as they dictate the material's performance in a given application. For instance, as a photocatalyst for H_2 evolution, p-Si is required to have high crystallinity and porosity and a low number of grain boundaries and oxygen content.[19] Opposingly, p-Si for battery anodes requires lower crystallinity with low to moderate surface area (Table 1).[35] With this in mind, it is essential to establish a synthetic route that is tunable and can easily produce p-Si with varying physical properties in addition to being scalable, simple, and inexpensive.

There are two main routes to synthesize p-Si: top-down (etching approaches) or bottom-up (chemical conversion approaches).[40] Both top-down and many bottom-up approaches initially require the production of non-porous, metallurgical grade Si through the carbothermal reduction method as seen in Fig. 2.[41] This is an energy intensive process that requires temperatures of >2000 °C in an electric arc-furnace to reduce SiO_2 using C as seen in eqn (1).[41,42] Along with metallurgical grade Si, SiC can also be obtained from the carbothermal reduction process.

$$SiO_{2(l)} + 2C_{(s)} \rightarrow Si_{(l)} + 2CO_{(g)} \quad \Delta H^{\circ}_{(25\,^{\circ}C)} = 695\ \text{kJ mol}^{-1} \quad (1)$$

Carbothermal reduction produces non-porous Si, which is further processed and refined through a variety of routes as

[a]Department of Chemistry, Dalhousie University, 6243 Alumni Crescent, Halifax, NS B3H4R2, Canada. E-mail: mita.dasog@dal.ca

[b]Department of Chemical and Biological Engineering, The University of Sheffield, Mappin Street, Sheffield S1 3JD, UK

† Electronic supplementary information (ESI) available. See DOI: https://doi.org/10.1039/d4sc04065a

‡ These authors contributed equally to this work.

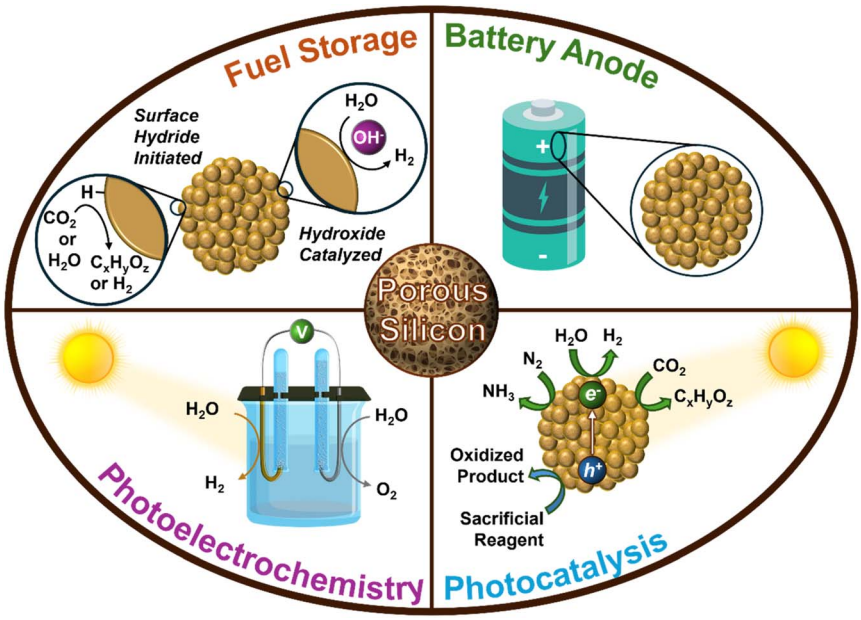

Fig. 1 Common uses of p-Si in energy storage applications.

Table 1 Summary of physical property requirements of p-Si nanostructures for various energy storage applications

	Energy storage application			
Properties	Battery anode material	Photocatalytic H_2 production	Photoelectrochemical H_2 production	Chemical H_2 storage
Crystallinity	Amorphous/low[2]	Moderate–high[36]	High[37]	Unknown
Surface area (m^2 g^{-1})	20–250 (ref. 2)	>150 (ref. 17 and 36)	Unknown[a]	5–580 (ref. 19 and 38)
Particle size	Nano[39]	Nano/micron[15]	Nano/micron[37]	Nano/micron[33]
Pore size	Meso[2]	Meso[36]	Meso[25]	Unknown

[a] Surface area is not commonly reported in this field.

shown in Fig. 2. This can be zone refined to produce transistor grade Si[41] and etched with HF acid to produce p-Si films[43] which can then be ball-milled to produce p-Si powders.[44] Alternatively, transistor grade Si or SiC can be chlorinated to produce $SiHCl_3$ and $SiCl_4$ (ref. 41) and further converted to SiH_4 through a catalyzed reaction at 50 °C.[45] These molecular precursors can then all be used for the chemical vapor deposition (CVD) process in the presence of a template to produce p-Si.[45–48]

As an alternative to high temperature, multistep processes to produce p-Si outlined above, metallothermic reduction reactions can use synthetic and natural SiO_2 sources as feedstock to form p-Si at comparatively low temperatures and in a single step. This gives metallothermic reductions an advantage in the form of feedstock flexibility and energy cost (which is demonstrated *via* calculations in ESI, Tables S1 and S2†).[49] We have estimated that starting at SiO_2, 1 kg of p-Si made by the MgTR process consumes 91 kW h (Fig. S2†), compared to 494 kW h *via* the Siemens process (Fig. S1†). The Ellingham diagram (Fig. 3) is an easy way to determine which metals are able to reduce SiO_2.[50] The reduction of SiO_2 involving Mg is called magnesiothermic reduction (MgTR) and is the most studied metal compared to the other options. Of all the metals that are able to

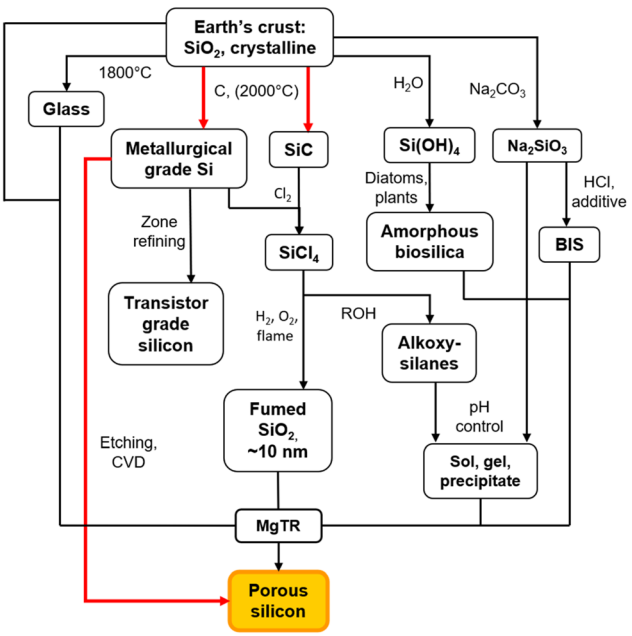

Fig. 2 Schematic of various routes and silica sources to produce p-Si. Red arrows indicate carbothermal reduction followed by etching to produce p-Si. Black arrows indicate the formation of various final silica products.

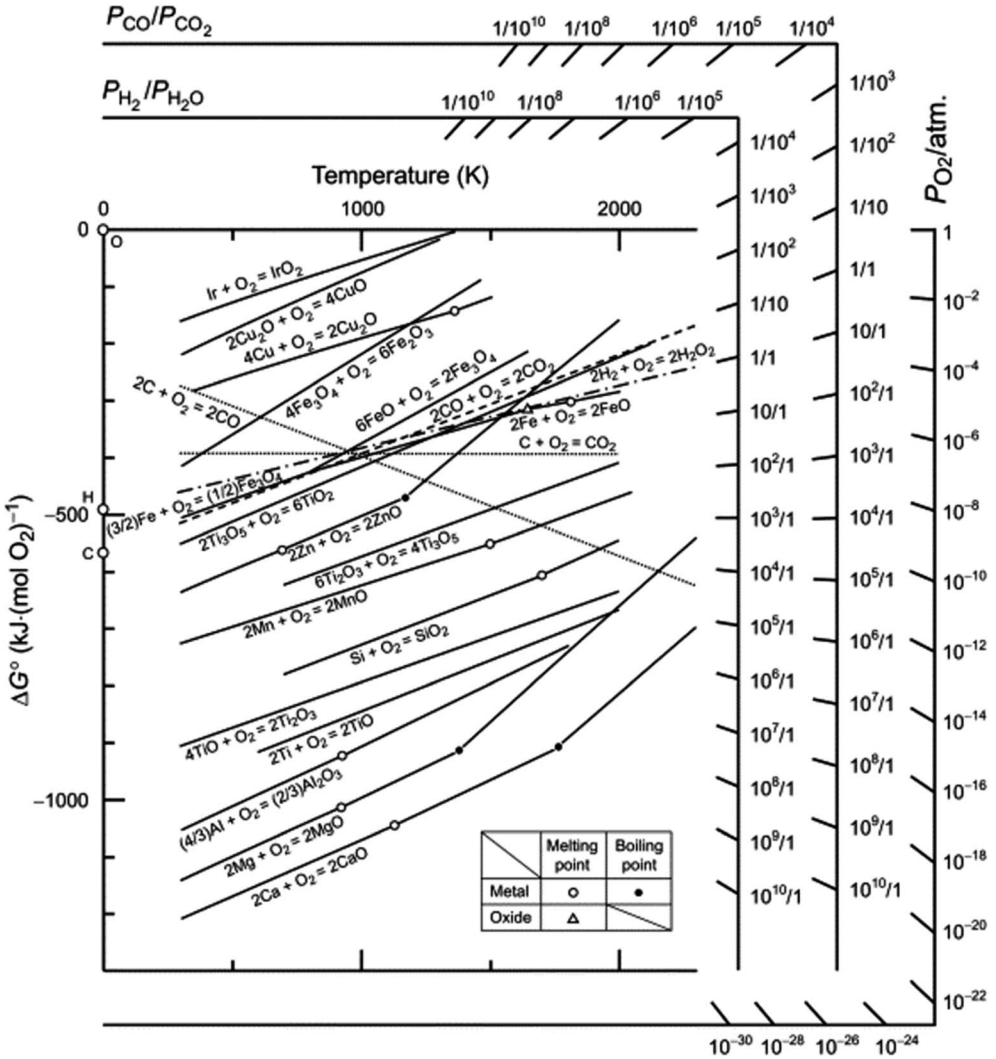

Fig. 3 Ellingham diagram of various oxides with Richardson nomographic scales included. This figure has been reproduced from ref. 50 with permission from Elsevier and Elsevier Books, Copyright 2014.

Table 2 Summary of important properties for potential reducing metals for metallothermic reduction

	Ca	Na	Al	Mg
Melting temperature (°C)[57]	840	98	660	650
Vapor pressure[a] (Pa)[51]	203	1.54×10^{-3}	3.48×10^{-7}	383

[a] Vapor pressure calculated at the melting point of the respective metals.

reduce SiO_2, Mg has one of the lowest bulk melting temperatures of 650 °C and is the most volatile, having a high vapour pressure at relatively low temperatures (0.5 Pa at 400 °C) enabling short reaction times at relatively low temperatures.[51] The by-product of the reaction, MgO, can be easily removed at room temperature using abundantly available acids.[52] Other metals such as Al, Ca, and Na have been used for the metallothermic reduction (Table 2). Ca has a relatively low melting point, high vapor pressure and high reactivity, making it a suitable reductant. The calciothermic reduction of SiO_2 has been reported once by Mishra *et al.* in 1985 where granular Ca was reacted with rice husks at 720 °C.[53] Na has also been explored for sodiothermic reduction at low temperatures due to its low melting point and reasonable (although lower) vapor pressure as seen in Table 2. A study by Wang *et al.* reduced the zeolite ZSM-5 using small pieces of Na metal.[54] The mixture was evacuated for 2 h then heated to 300 °C and held for 20 h. The resulting mixture was washed with HCl to remove the by-products and the Si formed was amorphous. Even though this reaction proceeds at relatively low temperature, the high reactivity of Na makes it difficult to handle on larger scales.[55,56] Aluminothermic reduction of SiO_2 is typically performed between 650 and 800 °C given that the melting point of Al is 660 °C as seen in Table 2.[55] The resulting product is highly crystalline, porous and has a high degree of morphological retention. Compared to MgTR, aluminothermic reduction produces p-Si with reduced porosity and lower surface area. This can be due to incomplete removal of the Al_2O_3 by-product which is

extremely difficult to remove.[55] MgTR is currently the favorable synthetic route that produces p-Si given the tunability, ease of handling, byproduct solubility and overall reactivity.

The MgTR reaction was first studied by Banerjee *et al.* in 1982 (ref. 58) and was revisited by Bao *et al.* over two decades later where they showed morphology retention using diatom frustules after reducing them with Mg at 650 °C for 2.5 h.[59] The principle of morphology retention is highly useful when producing complex p-Si structures with specific physical properties. However, to accomplish this, the reaction conditions must be carefully controlled. This is because MgTR is highly exothermic (eqn (2)), and the heat generated can lead to the collapse of pores and damage to the structure of the p-Si product.[28] The collapse of pores and particle sintering occur as internal temperatures have been reported to reach >1000 °C which approaches the Si melting point of 1414 °C.[60] Many efforts have been made to understand the mechanisms of the reaction to gain better control over the properties of the resulting p-Si. In this perspective we review the milestones in the understanding of the MgTR reaction and consider how understanding thermal management along with the reaction mechanism is key to the future of p-Si as an energy storage material. We discuss the techniques that have been employed to control the heat release of the reaction and the importance of thermal control when scaling up the reaction.

The MgTR mechanism

MgTR is typically performed between 500 and 950 °C for <20 hours to ensure complete reduction of SiO_2 (Fig. 4A).[2] The reduction of SiO_2 to Si is hypothesized to occur with Mg in the vapor phase and is highly exothermic (eqn (2)).[59]

$$SiO_{2(s)} + 2Mg_{(g)} \rightarrow 2MgO_{(s)} + Si_{(s)} \quad \Delta H^{\circ}_{(650\ ^{\circ}C)} = -619.9\ \text{kJ mol}^{-1} \tag{2}$$

MgO is produced as a by-product which can be easily removed by treating with an acid such as HCl, to form water soluble $MgCl_2$ which can be easily washed away. However, other reactions can occur during MgTR such as the formation of Mg_2Si (eqn (3)). This is the major side reaction of MgTR and is generally favored when excess Mg is present.[62]

$$Si_{(s)} + 2Mg_{(g)} \rightarrow Mg_2Si_{(s)} \quad \Delta H^{\circ}_{(650\ ^{\circ}C)} = -350.3\ \text{kJ mol}^{-1} \tag{3}$$

An *ex situ* analysis performed by Yoo *et al.* at different stages of the MgTR reaction showed that within the first 10–20 minutes of the reaction, there is a high concentration of Mg_2Si.[63] It is expected that Mg_2Si forms at the beginning of the reaction when there is a high concentration of Mg vapor according to eqn (4). As the reaction progressed, Mg_2Si disappeared, suggesting that it's an intermediate rather than an unwanted by-product.[63] The disappearance of Mg_2Si is presumed to be due to the reaction of Mg_2Si with SiO_2 (eqn (5)) since the interface between Mg_2Si and SiO_2 is unstable, as shown by the lack of a stable tie-line in the Mg–O–Si phase diagram in Fig. 4B. From the phase diagram, it is clear that only MgO and Si can form stable interfaces with SiO_2. If the reaction conditions are not carefully chosen, unreacted Mg_2Si within the reaction product will react with HCl during the acid washing step to form SiH_4 which ignites in air, reforming SiO_2.[64] This causes a safety hazard and reduces the yield of elemental Si.

$$4Mg_{(g)} + SiO_{2(s)} \rightarrow Mg_2Si_{(s)} + 2MgO_{(s)} \quad \Delta H^{\circ}_{(650\ ^{\circ}C)} = -1308.2\ \text{kJ mol}^{-1} \tag{4}$$

$$Mg_2Si_{(s)} + SiO_{2(s)} \rightarrow 2Si_{(s)} + 2MgO_{(s)} \quad \Delta H^{\circ}_{(650\ ^{\circ}C)} = 68.4\ \text{kJ mol}^{-1} \tag{5}$$

Another side reaction that can occur during MgTR is the formation of Mg_2SiO_4 and $MgSiO_3$, as seen in eqn (6) and (7). The formation of Mg_2SiO_4 and $MgSiO_3$ is parasitic and reduces

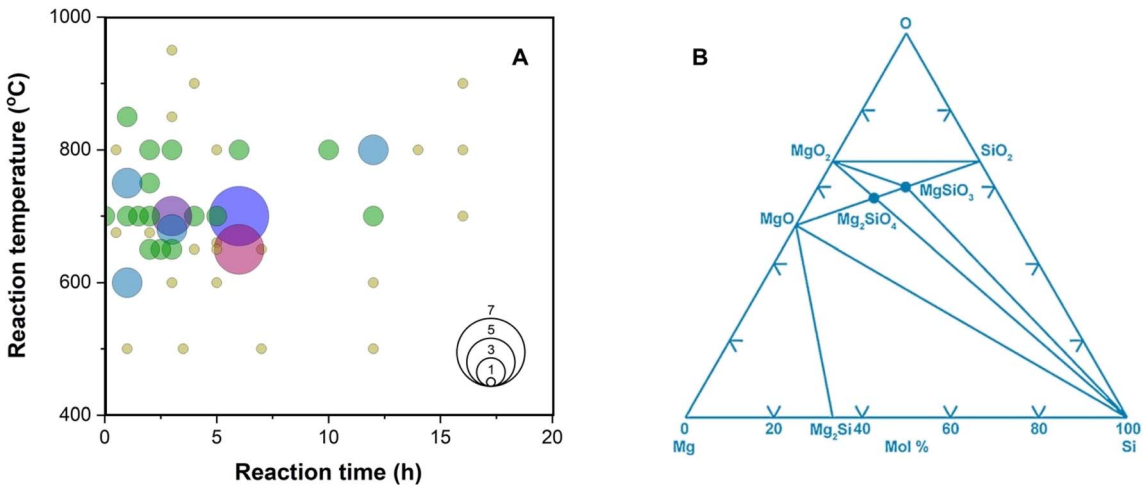

Fig. 4 (A) Temperature and time profiles used in literature sources (summarized in Table S1†). The size of the circle represents the frequency of the reaction conditions used. (B) Calculated Mg–Si–O phase diagram at 25 °C. This figure has been adapted from ref. 61 with permission from Elsevier, Copyright 2006.

the yield of Si. Even though MgO–Si and MgO–SiO_2 systems seem to be stable at room temperature (Fig. 4B), Kamitsuji *et al.* found that reactions between MgO, Si and SiO_2 occur at temperatures >800 °C to form silicates.[65] More specifically, Brindley *et al.* proposed that the temperature at which Mg_2SiO_4 is formed ranges from 1100–1400 °C.[66] The silicates tend to form when two conditions are satisfied: (1) when there is insufficient Mg and (2) when there is high heat buildup in the system.[2] The most likely place for this to occur is at the interface of SiO_2 and MgO. Unfortunately, the silicates are highly stable and cannot be easily removed *via* chemical treatment. Additionally, they have been reported to have a negative effect on the Si material for use in battery anodes.[67]

$$SiO_{2(s)} + 2MgO_{(s)} \rightarrow Mg_2SiO_{4(s)} \quad \Delta H^{\circ}_{(650\,^{\circ}C)} = -15.0\ \text{kJ mol}^{-1} \tag{6}$$

$$SiO_{2(s)} + MgO_{(s)} \rightarrow MgSiO_{3(s)} \quad \Delta H^{\circ}_{(650\,^{\circ}C)} = -3.9\ \text{kJ mol}^{-1} \tag{7}$$

While various reaction products have been observed during MgTR as shown in eqn (2)–(6), the sequence of reactions and factors affecting them have not been understood in detail. The mechanism for MgTR has been the subject of investigation as its deep understanding can help choose appropriate reaction parameters to avoid the formation of unwanted products and to achieve the desired physical properties for energy storage applications.[67] It is agreed in the literature that the reaction occurs through the diffusion of Mg vapor into SiO_2 resulting in a matrix of MgO and Si.[2] Gutman *et al.* performed a mechanistic study on a thin glass slide and had observed that the growth rate of the product layers (Si/MgO and Mg_2Si) decreased with time.[61] This phenomenon follows the parabolic law and confirms that the MgTR reaction is a diffusion-controlled process. Since MgO is dispersed throughout the Si products, its removal *via* acid treatment yields the porous structure. Furthermore, Gutman *et al.* discovered that the product (reaction zone) consisted of periodic layers of Mg_2Si and Si/MgO rich zones after a reduction reaction with temperatures ranging between 400 and 650 °C.[61] This layered structure is formed through the long-range diffusion of Mg atoms to SiO_2 and short-range diffusion of Si atoms from SiO_2 to the SiO_2/MgO interface (Fig. 5). Si was not observed in this layered structure using the scanning electron microscopy (SEM) technique in this study due to the presence of a vast excess of Mg (glass slide was immersed in Mg powder) favoring the formation of Mg_2Si. While this study showed the relative diffusion of various atoms during MgTR, it isn't reflective of typical reduction conditions which utilize Mg : SiO_2 ratios of 2–2.5 : 1.

Rasouli *et al.* found that the MgTR reaction proceeds *via* a shrinking core model, limited by the amount of Mg present in the reaction.[68] Different microstructures of the product Si/MgO/Mg_2Si matrix were formed depending on the mole ratio of Mg : SiO_2. Through backscattered electron imaging, a layer of Si and MgO was observed on the surface of the quartz particle. Unreacted SiO_2 remained at the center since a sub stoichiometric mole ratio of 1 : 1 Mg : SiO_2 was used. At a 2 : 1 mole ratio the core shrunk while the surrounding MgO/Si layer grew thicker. At 3 : 1 and 4 : 1 mole ratios, the quartz particles had cracked into smaller pieces due to the penetration of unreacted Mg liquid into the SiO_2 particles.[68] It should be noted that a higher reaction temperature of 1100 °C was used in this study which is not typical of MgTR (Fig. 4A). More recently the MgTR mechanism was investigated by Martell and Yan *et al. via* in-

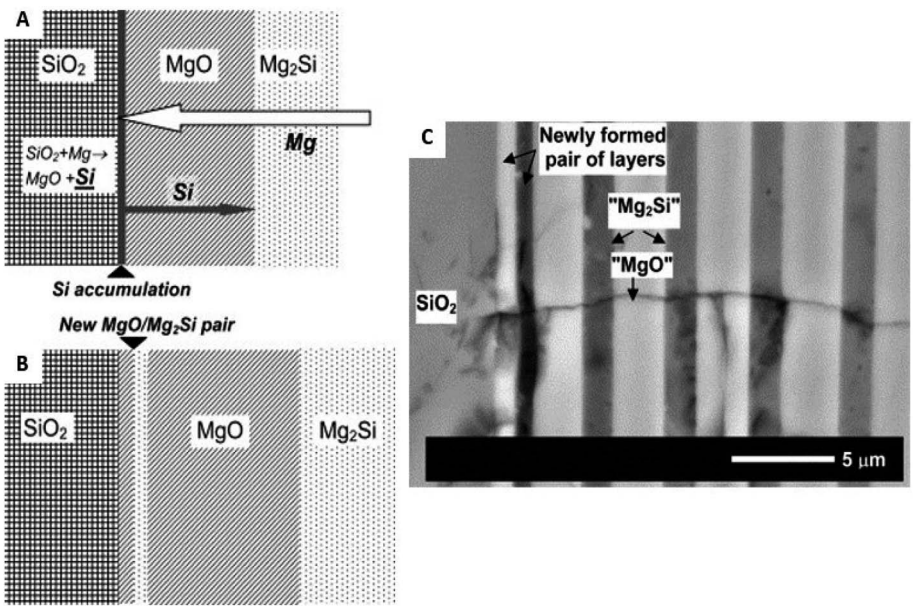

Fig. 5 Description of the periodic layer mechanism as explained by Gutman *et al.*: (A) Si atom accumulation at the SiO_2/MgO interface as a result of poor Si atom diffusion; (B) simultaneous formation of a new MgO/Mg_2Si pair of layers. (C) Cross sectional backscattered electron scanning electron microscopy image (SEM) of a new MgO/Mg_2Si pair of layers formed at the SiO_2 interface during annealing at 450 °C (after 168 h). This figure has been reproduced from ref. 61 with permission from Elsevier, Copyright 2006.

operando powder X-ray diffraction (XRD) studies.[69] The studies revealed that the reaction onset temperature is Mg particle size dependent and lower than what was proposed previously (*e.g.*, 348 ± 7 °C for 22 μm Mg particle size). It was observed that amorphous Si forms first according to eqn (2) and is immediately converted to Mg_2Si *via* eqn (3). Crystalline Si forms above 550 °C *via* reaction (4) thus confirming that silicide is an important intermediate during MgTR and not a byproduct that forms just in the presence of excess Mg. In addition to revealing the reaction mechanism, the study also demonstrated that thermal management is an extremely important aspect of MgTR. The type of precursors and reaction conditions (set temperature, time, ramp rate, *etc.*) affect the rates of the reactions involved within the mechanism and the amount of heat released within a given time frame. Thus, we will discuss the impact of heat on the reaction as well as approaches to manage it.

Crucial factors affecting the thermal behavior of reactions

Ramp rate

Heating rates ranging from 1–40 °C min^{-1} have been used in MgTR, although the majority of the studies ramp the reaction between 5 and 10 °C min^{-1}.[2] The fast ramp rates result in a rapid release of heat in a given time frame due to the exothermic nature of many of the reactions involved (Fig. 6A). If there is insufficient time for the heat to dissipate throughout the reaction mixture, it can lead to high local temperatures (>1000 °C), leading to particle sintering, loss of morphology, lower surface area, larger crystallite sizes and silicate formation.[2] A study by Shi *et al.* investigated heating rates of 5, 3 and 1 °C min^{-1} while reacting SiO_2 from rice husks with 200 mesh Mg (74 μm).[6] In the 5 and 3 °C min^{-1} reactions, Mg_2SiO_4 was detected indicating signs of heat accumulation since silicate formation is favored above 1000 °C despite the set temperature being 650 °C. Opposingly, no Mg_2SiO_4 was detected when a ramp rate of 1 °C min^{-1} was used. The surface areas for the SiO_2 and 1, 3 and 5 °C min^{-1} Si samples were 221 m^2 g^{-1}, 267 m^2 g^{-1}, 12.6 m^2 g^{-1}, and 7.5 m^2 g^{-1}, respectively.[6] The 1 °C min^{-1} sample had mesopores (10–20 nm) whereas the 3 and 5 °C min^{-1} samples had very few pores, most of which were within the macro-size regime. It was proposed that with higher ramp rates, the heat accumulation becomes so severe that it causes the MgO crystallites to grow rapidly and Si to sinter.[6] As the pores are formed due to the removal of MgO, large crystallites result in macroporous Si with low surface area, high crystallinity but low purity. However, utilizing slow ramp rates prolongs the reaction time making it an unattractive option when scaling up due to economic and energy considerations.[70]

Precursor particle size

Focusing on the SiO_2 particle size, Yan *et al.* found that the cutoff temperature for the reaction to proceed was dependent on the

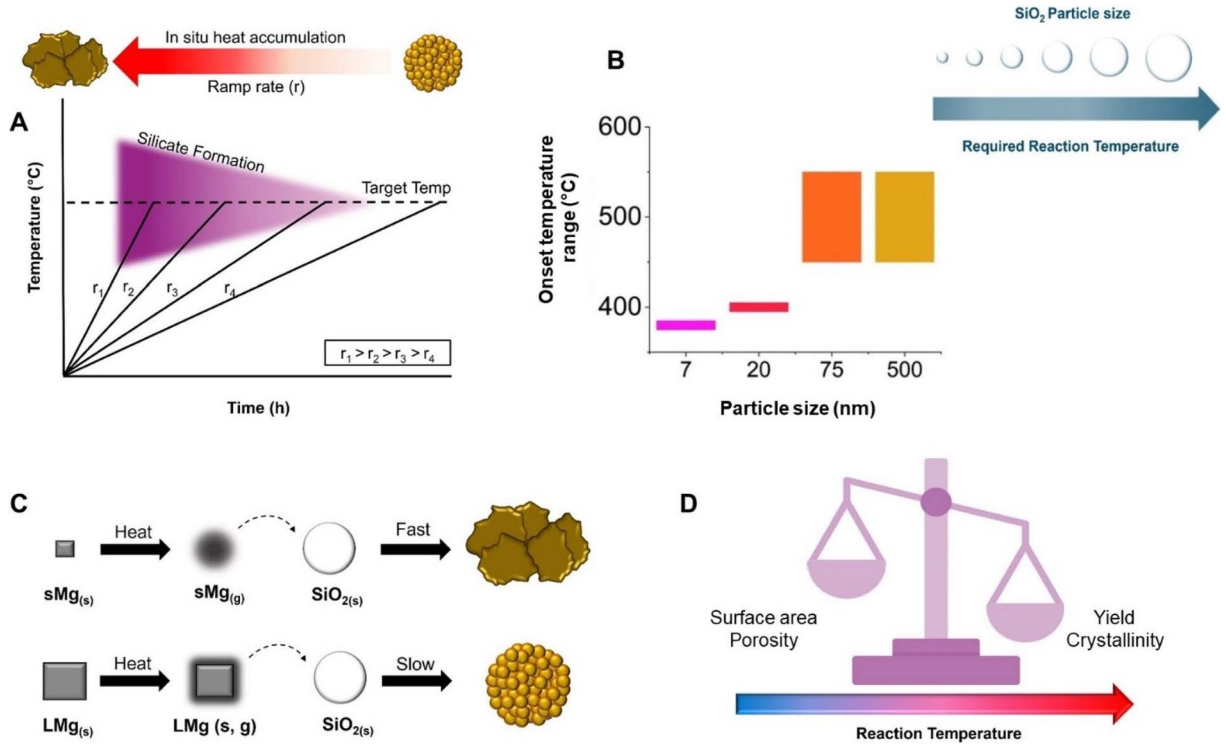

Fig. 6 (A) Schematic of the influence of the ramp rate on silicate formation, and heat accumulation with respect to ramp rate. (B) Change in reaction onset temperature as a function of SiO_2 size. This figure has been adapted from ref. 71 with permission from the Royal Society of Chemistry, Copyright 2021. (C) Mg particle size effect on heat accumulation in the reaction system and its influence on reaction kinetics and the resulting p-Si product. (D) Schematic of reaction temperature and how it relates to crystallinity, surface area, porosity and Si yield.

SiO_2 particle size.[71] Fumed SiO_2 (fractal aggregates of 7 nm primary particles), and Stöber SiO_2 of 20 nm, 75 nm and 500 nm were used in this study. It was found that 7 nm particles were able to react at the lowest temperature of 380 °C with a yield of 60%. The 20 nm particles reacted at 400 °C, resulting in a yield of 38% Si, while the 75 and 500 nm particles did not form any Si below 450 °C (Fig. 6B). This study has implications for the thermal management of the reaction, whereby a runaway reaction can more easily be avoided if the temperature is kept low. While the study shows that it is possible to reduce SiO_2 at temperatures below 400 °C, the mechanism for the reaction at these temperatures is still unknown and requires further study. Other than the effect on reaction yield, the effect of the SiO_2 size on porosity, surface area and crystallinity has not been systematically studied.

A study by Yang *et al.* examined the influence of Mg particle size on the reduction of synthesized SiO_2 spheres at 650 °C at a ramp rate of 10 °C min^{-1}.[3] When Mg particles of 44 and 74 μm were used, the reaction produced heat rapidly, leading to morphological destruction as well as the formation of Mg_2SiO_4. However, when larger Mg particles (>800 μm) were used, the Si product had the same spherical morphology as the SiO_2 precursor and no Mg_2SiO_4 was detected. The specific surface areas for the small, medium and large sized Mg samples were 70.6, 56.8 and 223.3 m^2 g^{-1}, respectively.[3] As Mg particles get smaller, they vaporize faster and are more reactive.[72,73] When using particles with high innate reactivity, the reaction will be initiated at a lower temperature and the reaction wave will spread rapidly, producing a large amount of heat in a short amount of time.[3] As the Mg particle size increases, Mg will vaporize slowly and the rate at which it reacts decreases which leads to a decrease in the amount of heat accumulated (Fig. 6C).[3] Martell and Yan *et al.* showed that the Mg particle size has an effect on reaction onset temperature and product distribution.[69] Large Mg particles (100 μm) led to a sustained feed of Mg vapour, which favoured the production of Mg_2Si, and hindered its consumption. As a result, Mg_2Si persisted for a longer duration compared to when smaller Mg particles (45 μm) was used. The onset of its conversion back into Si was delayed by about 25 minutes at 650 °C for the larger Mg particles. However, faster and smaller Mg particles without heat management lead to the formation of highly crystalline and sintered Si which can be deleterious for both battery and photocatalytic applications.[34,36]

Reaction temperature and time

Key parameters that affect all chemical reactions are temperature and time. The outcome of MgTR at different reaction times and temperatures was studied by Entwistle *et al.* who showed that at 650 °C, the yield, specific surface area and porosity of Si did not change beyond 1 hour.[34] Although hold times above 1 hour have no impact on the resulting Si at 650 °C, it may have an impact on reactions performed at lower temperatures which require more time for sufficient Mg diffusion through the reaction products or when less reactive Mg is used. A study by Martell and Yan *et al.* found that for MgTR at lower temperatures, longer reaction times are required to fully convert the Mg_2Si intermediate back to Si *via* eqn (5).[69] For example, at 450 °C the Mg_2Si intermediate required 51 min to convert back to Si; however at 650 °C it only took 22 min. Additionally, when less reactive, larger sized Mg was used at 650 °C, the Mg_2Si intermediate required 90 min to fully convert.

In terms of the reaction temperature, Entwistle *et al.* found that higher set values resulted in a higher Si yield.[34] This finding is in agreement with an earlier study presented by Gutman *et al.*,[61] which showed that the reaction mechanism is governed by mass diffusion of Mg through the MgO and Mg_2Si layers. The rate of diffusion is determined by the temperature and concentration of Mg, of which the latter depletes with time, thereby decreasing the rate of diffusion. Furthermore, reduction of SiO_2 ceases as Mg is unable to diffuse through the MgO and Mg_2Si layers to reach unreacted SiO_2. As the temperature increases, so does the rate of diffusion, and Mg can penetrate through these layers to reach SiO_2. The formation of Si is also favored at higher temperatures (>850 °C) due to the conversion of Mg_2Si back into Si *via* reaction (5).[34] This was confirmed by a study performed by Yoo *et al.*, that showed that Mg_2Si was formed within 10 min of the reaction reaching 680 °C.[63] As the reaction proceeded, Mg_2Si was consumed while Si was formed, all within 25 minutes of reaching 680 °C. Entwistle *et al.* demonstrated that as reaction temperature increases, the crystallite size of the primary Si particles also increases which leads to a reduction in specific surface area and porosity. For example, the average crystallite size of the primary Si particles was found to increase from 5 to 48 nm when changing the reaction temperature from 550 to 950 °C due to sintering of the Si.[34] With this in mind, choosing a reaction temperature is a balance between Si yield, crystallinity, and its porosity (Fig. 6D). Furthermore, if Mg_2Si is observed in the reaction product, its complete conversion to Si can be ensured by increasing either the reaction time (if using smaller Mg) or temperature (with larger Mg particles).

Reaction molar ratio

While a 2 : 1 stoichiometric molar ratio of Mg : SiO_2 is required for the reaction to occur, a slight excess of Mg is typically used to push the reaction towards completion and account for surface oxide on Mg particles. In most MgTR reactions, Mg : SiO_2 molar ratios range from 2.2 : 1 to 2.5 : 1. When utilizing substoichiometric mixtures, the reaction favors the formation of magnesium silicates,[68] but this can be avoided by using lower reaction temperatures.[61] However, this will result in low Si yield due to incomplete reduction. A multi-step reduction method was recently reported, where in each step the amount of Mg added was substoichiometric, until a 2 : 1 molar ratio was reached.[74] This resulted in controlled reactivity and avoided heat accumulation which gave smaller crystallites of Si. An alternative MgTR known as "deep reduction" has recently been reported which uses a Mg : SiO_2 ratio of 5 : 1.[62,75] When using such high amounts of Mg, the major reaction product is Mg_2Si which is then converted into Si and SiO_x *via* air oxidation. While mixtures of Si and SiO_x have been shown to be good for battery applications,[76,77] the formation of oxide can be detrimental to photocatalytic and fuel production reactions.[17,36] Furthermore,

technoeconomic analysis has shown that higher Mg : SiO_2 ratios increases the Si production cost.[70]

As discussed in this section, many reaction parameters affect the physical properties and yield of Si during MgTR. While porosity and crystallinity of the reaction product are typically well characterized and summarized, the link between different reaction conditions and Si yield has not been reported widely or accurately for two reasons. Firstly, hydrofluoric acid is often used to remove unreacted SiO_2, so the yield measurement is not representative of the reaction progress. Secondly, the most common method for measuring yield is X-ray photoelectron spectroscopy, which is a surface technique, and therefore not representative of reaction progress in the whole sample. Analytical methods such as thermo-gravimetric and elemental oxygen analysis methods are the most accurate but rarely reported. Therefore, researchers should consider reporting Si yields using these or similar techniques in the future to gain better understanding of MgTR.

Thermal management

MgTR is highly exothermic as seen in eqn (2) and without proper thermal management, it leads to particle sintering and low surface area.[78] This results in a p-Si product that has low photocatalytic activity due to carrier recombination at the grain boundaries[36,79] and low fuel conversion yields in stoichiometric reactions due to low surface area.[28] The high amounts of heat also result in crystalline Si which is not ideal for battery applications due to the mechanical fracture caused by volumetric expansion of larger crystallites.[80] A study by Zhang *et al.* investigated the heat released in the MgTR reaction by inserting a K-type thermal-couple connected to a data acquisition unit into the reaction mixture.[60] The study showed that when the powder mixture is heated at a rate of 5 °C min^{-1}, the temperature increases linearly up until 465 °C. After reaching 465 °C the temperature started to increase at a faster rate until it reached 535 °C (10 min later) after which it spikes to 1270 °C within 20 s. This study suggests that the onset of the reaction is around 465 °C and the most exothermic reactions are completed within about 20 min (the time it took for the temperature to re-equilibrate).[60] As *in situ* temperatures approach the melting point of Si (1414 °C), particle sintering can occur which results in a loss of surface area and destruction of precursor architecture.[3,81] Additionally, at high temperatures, Mg_2SiO_4 is formed which decreases the final yield of Si.[6] This is a major issue which complicates scaling up of MgTR since the thermal runaway is more pronounced in large batches due to slow heat transfer.[2] The proposed methods of controlling the reaction temperature include decreasing the heating ramp rate, increasing the Mg particle size, decreasing reaction temperature, separating SiO_2 and Mg reagents, and utilizing a heat sink.[60] Many of these have been demonstrated to be effective at providing thermal management and will be briefly covered in this section.

Controlled Mg feed

A study by Xie *et al.* used a custom reaction boat to investigate whether separating the Mg and SiO_2 precursors would help avoid excess heat production.[82] A stainless-steel cylinder with a holey plate in it (Fig. 7A top), separating the top and bottom half of the reactor was built. SiO_2 was placed on the top level whereas Mg powder was placed on the bottom. As the reactor was heated to 700 °C and held for 12 h, Mg vaporized and reacted with the SiO_2 above it.[82] The final Si product contained Mg_2SiO_4 due to insufficient Mg vapor interacting with the SiO_2. To relieve this issue, the temperature was increased to 800 °C, which yielded Si without any detectable Mg_2SiO_4.[82] The downside to this approach is that it requires high temperatures (>650 °C) as well as long reaction times. Additionally, since the Mg is not intimately mixed with the SiO_2, some Mg vapor may be

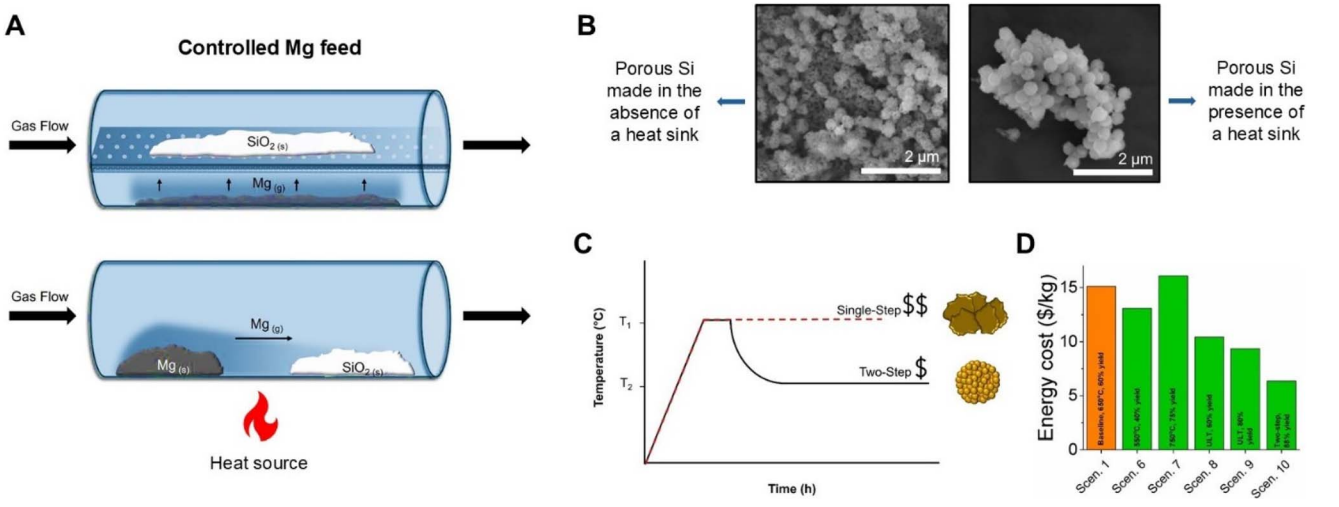

Fig. 7 (A) Schematic of the controlled Mg feed with a holey reaction container (top) and Mg positioned "up-stream" of the SiO_2 (bottom). (B) Scanning electron microscopy images of porous Si particles made in the absence and presence of a heat sink. (C) Two-step *versus* single-step reaction conditions. (D) Cost comparison of reaction conditions with the two-step condition being scenario 10, variations of ultra-low temperature (ULT, 380 °C) being scenario 8 and 9, reaction at 750 °C being scenario 7, and variations of reactions at 650 °C being scenario 1 and 6. (C) is reproduced from ref. 70 with permission from Elsevier, Copyright 2023.

removed from the system by the carrier gas potentially resulting in inhomogeneity in the reaction product. Another approach was utilized by Bao *et al.* where Mg and SiO_2 were kept on separate ends of the reaction container rather than incorporating a mixing step (Fig. 7A bottom),[59] and the reactants were heated to 650 °C for 2.5 h. Unfortunately, with this method, incomplete reduction of SiO_2 was observed. The reaction product contained three regions of different species that were different in color (blue/brown/white). The region of the product closest to the Mg source was found to be Mg_2Si, the center was Si and the region farthest from the Mg source was unreacted SiO_2.[59] While this approach may reduce the heat accumulation by controlling the Mg vapor feed, the way it is currently implemented results in a variety of reaction products due to insufficient reactant mixing. In the future, adding a rotary aspect, specifically to the SiO_2 reactant zone may be required to obtain a homogeneous reaction product.

Eutectic reductants

Another route for reducing the heat released within a short period of time is to use lower reaction temperature without compromising the yield. Since Mg metal has a high vapor pressure, reactivity of the mixture can be decreased by forming a eutectic with an additional metal with a lower vapor pressure that can reduce SiO_2. For example, the Mg–Al binary phase diagram reveals that a eutectic can be made at a composition of 66.7 at% Mg and 33.3 at% Al which has a melting point of approximately 437 °C.[55,83] Adding Al can help lower the reaction rates and amount of heat accumulated and reduce the amount of Mg required. The eutectic mixture of Al and Mg has been studied by Lai *et al.*, where a 70% Mg and 30% Al mixture reacted at 450 °C for 12 h was found to yield Si with retained precursor morphology, a moderate surface area of 132 $m^2\ g^{-1}$ and average pore diameters of 8 nm.[84] A Ca/Mg eutectic is also worth exploring as Ca is highly abundant, and is able to reduce SiO_2.[67,83] Although choosing two metals that are able to reduce SiO_2 has been explored, using eutectic mixtures of Mg and another non SiO_2 reducing metal such as Sn or Zn would allow for the reaction to be performed at lower temperatures (Table 3) if they minimize the Mg vapor pressure.[83]

Heat sinks

Heat sinks are one of the more popular methods of controlling the excess heat accumulated during MgTR. These are typically inorganic salts that are added to the reaction mixture to absorb excess heat and help prevent morphological damage and sintering (Fig. 7B).[84] The chosen salt must have a high heat capacity, thermal conductivity, and thermal stability, be inexpensive, and remain chemically inert during the reaction. Examples of salts used are NaCl, $MgCl_2$, $CaCl_2$, KCl, and NaBr.[84] A study by Khanna *et al.* compared multiple inorganic salts as heat sinks and found $CaCl_2$ to be the best performing heat sink as it produced high surface area p-Si with the least amount of structural damage and sintering. $MgCl_2$ was also found to perform well as a heat sink and is less expensive than $CaCl_2$. NaCl is one of the most commonly used heat sinks in the literature; however, $CaCl_2$ and $MgCl_2$ have been reported to better prevent sintering and morphological damage compared to NaCl.[84] After the reaction, the salt is easily removed through aqueous washing steps. Although NaCl is not the best performing heat sink, its efficacy can be improved by adding it in large excess. The study by Zhang *et al.* previously mentioned at the beginning of this heat control section attempted to reduce the temperature spike of 1270 °C by adding NaCl to the reaction mixture at a SiO_2 : NaCl molar ratio of 1 : 5.[60] When NaCl was added to the reaction, the initial reaction onset temperature increased from 465 to 535 °C and the exothermic temperature spike decreased from 1272 to 792 °C. When using molar ratios that were less than 1 : 5, the exothermic temperature spike was not successfully kept below 1000 °C. Through this study it is clear that heat sinks do effectively prevent heat accumulation when added in large amounts. Unfortunately, it is an additional reagent which is required in large excess and increases the complexity and overall cost of MgTR.

Table 3 Summary of eutectic mixtures with Mg and their associated melting points

Eutectic mixture (at%)	Melting point (°C)
Mg–Ca (11)[83]	520
Mg–Sn (11)[83,85]	567
Mg–Al (33)[55]	432
Mg–Li (30)[86]	592
Mg–Zn (29)[83]	342
Mg–Ni (11)[83]	511
Mg–Cu (16)[83,84]	487

Two-step reduction

A modified thermite method can be used to regulate the exothermic nature of MgTR and use the released heat to propel the reaction further. A study by Martell *et al.* used this approach to reduce Stöber SiO_2 nanoparticles *via* MgTR.[28] The reaction mixture was initially heated to 650 °C to initiate it but the bulk of the reaction was performed at a second lower temperature (300 °C). This produced the highest surface area p-Si synthesized from a nonporous precursor. Furthermore, technoeconomic analysis has shown this to be the most cost and energy efficient MgTR pathway.[70] However, it should be noted that the first and second step temperatures are dependent on the precursors chosen and reaction quantity and need to be optimized for each system. This is time consuming and there are currently no high throughput systems to perform such screening.

Future outlook

The field of sustainable energy is growing fast, which drives the need for the production of energy storage and conversion materials. p-Si is amongst these materials, which makes MgTR a reaction of importance as it can convert SiO_2 to Si in a single reaction step. This reaction is a bulk processing method, can use natural and synthetic feedstock, and can be performed at

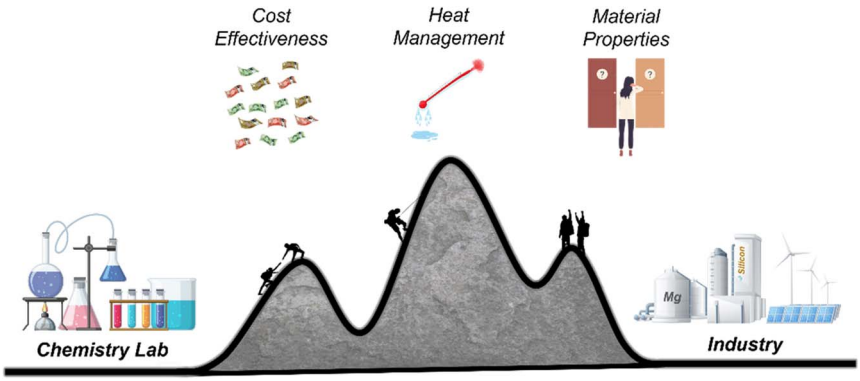

Fig. 8 Schematic representation of challenges that need addressing to scale up the MgTR process.

lower temperatures compared to conventional carbothermal reduction. The by-products can be removed easily using an acid, forming soluble salt and water. These features make the MgTR reaction a highly attractive option from a process design and scale-up standpoint. However, there are still outstanding challenges that need to be addressed to ensure its commercial success. They include (i) lack of a comprehensive, predictive model and (ii) lack of understanding of reaction behaviour beyond the lab-scale (10–100 s of grams). While addressing these challenges to develop the MgTR process (Fig. 8), it is important to maintain a holistic/system-level view, ensuring that multiple critical criteria are optimised simultaneously. Factors to consider include the performance, scalability, environmental impact and cost benefits as detailed elsewhere.[87] We should be cautious of not overindulging in a single parameter (*e.g.* structure, purity or surface area) in order to not hamper the overall development of this technology.

While MgTR has been widely studied, only a handful of systematic studies exist. Further systematic studies such as on the effect of SiO_2 particle size on the reaction mechanism and yield will allow more accurate predictions of the reaction outcome under given conditions. In the chemical industry, machine learning is making a huge impact, aiding engineers in recognising patterns and making predictions.[88] Tang *et al.* demonstrated for the first time the application of machine learning to MgTR, using data from previous studies to deduce a more accurate model to describe MgTR.[89] While it is still early days for machine learning in MgTR, more complete data sets will accelerate the growth of this field and make it an indispensable tool in accurately predicting the progress and outcome of the reaction.

Systematic studies need to be performed to address various challenges associated with reaction scale-up. The first challenge concerns the mixing of the reactants. Increasing the amount of p-Si production will naturally increase the volume of powder added to a kiln/furnace. The likelihood of inhomogeneity within the mixture increases with volume, which lead to mass transfer limitations, formation of excess Mg_2Si or silicates ($MgSiO_3$ and Mg_2SiO_4) and as a consequence, low Si yield. Inhomogeneity can be overcome by adapting proper mixing techniques. While proper mixing is easily achieved on a small scale using a mortar and pestle, it becomes unfeasible to mix powders by hand for mixtures beyond approximately 10 g. This process becomes physically laborious and inconsistencies in mixing can arise between different batches due to human factors. The mixing process should be automated to minimise inconsistencies, using equipment such as low-energy mills or tumblers and the effect of different types of mixing on the reaction and product properties should also be explored. A second challenge with scaling up involves thermal management. While heat can dissipate at the surface of a reaction mixture, the powder underneath is thermally insulated, causing the heat to build up. While salts act as effective thermal moderators, they are commonly used at mass ratios exceeding 1 : 1 salt : reaction mixture.[90] This means that majority of the space in the furnace/kiln is occupied by an inert material. In order to maximise throughput, it is essential that the mass of the heat sink is minimised, while still preventing sintering of the p-Si. Additionally, adding salt would increase the amount of water required in the acid treatment step to ensure its complete removal. Other methods of absorbing heat should be explored, such as the use of a heat sink that can easily be separated from the reaction mixture and reused. Thermal masses such as stainless-steel balls or rods could be used to not only absorb heat but also to aid with the mixing during the reaction. These can be easily separated from the powder mixture without additional water use and can be reused frequently.

Another way to achieve heat dissipation is by agitating the mixture during the reaction. This can be done using a rotary furnace, a common piece of equipment in materials processing, whereby powders are mixed through tumbling action while reacting at high temperatures. MgTR was carried out in a rotary furnace by Yoon *et al.*, and it was shown that the reaction yield could be increased with the rotational speed of the furnace.[91] The authors reported that the increase in rotational speed limited the formation of side products by improving heat and mass transfer. As the MgTR reaction is a bulk reaction, the rate of production, or amount produced in a single batch is determined by the volume of the furnace. By utilizing a rotational furnace, the process can transition from a batch to a continuous process. A rotating tube tilted on an angle would cause the powder to move from one end to the other. Adjusting the tilt of

the furnace would allow the user to change the time taken to travel from one end of the furnace to the other, exposing the mixture to cooler zones and hotter zones for different times. In this way, the ramp rate, dwell time and cooling rate can be controlled.

Another interesting route for MgTR is utilizing mechanical activation rather than thermal activation. Cho *et al.* demonstrated a magnesio-milling process in a planetary ball mill which yielded p-Si with meso- and macropores as well as high crystallinity.[14] They were able to scale up the magnesio-milling process to a 5 L attrition mill which utilized rotating balls and rods for mixing. The resulting p-Si had a relatively low surface area of 38.57 $m^2 g^{-1}$ and a large average crystallite size of 81 nm. Additionally, the SEM images reveal sintered Si which indicates that the excess heat is not sufficiently controlled *via* a standard magnesio-milling process. To sufficiently control the heat release, other thermal moderation techniques such as the ones discussed in this perspective should be employed in tandem with the milling.

The experimental MgTR conditions in the lab are predominantly chosen to produce p-Si with a desired set of properties while scale-up and industrial production requires that the conditions chosen for the reaction also be economically feasible. It is therefore important that in order for MgTR to move from the benchtop to an industrial setting, future studies should be guided by the techno-economics of the process. The ideal economical scenario for the reduction step is one which achieves the highest yield of Si at the lowest temperature in the shortest reaction time. This means striking a balance between yield, heating/cooling times, maximum temperature, and ramp rates. Each of these reaction parameters will affect the properties and performance of the final product. To study all these conditions and correlations will require an infinite number of experiments, and therefore, research efforts should focus on first studying and optimising the parameters which would have the greatest effect on process economics. Technoeconomic analysis performed by Yan *et al.* has shown how various conditions used in MgTR affect the overall cost of the process.[70] From an energy-cost perspective, minimising the dwell time at the maximum temperature is likely to have the greatest effect, followed by lowering the reduction temperature. The techno-economics should also be viewed from a process level, and how changing one step in the process affects the step before and after it. For example, if it is found that mixing in a rotary furnace alone is sufficient to facilitate the complete conversion of SiO_2 to Si, and this can eliminate the cost of equipment required to pre-mix the feedstock. Lowering the amount of salt means an increased throughput in the furnace and lower demand on downstream processing.

Conclusions

The wide range of uses of p-Si as an energy storage material drives the demand for this to be produced with varying properties and at different scales. While MgTR is considered the most promising process for scale-up, further work is needed to understand the behaviour of the reaction, address the challenges at intermediate scales and bridge the gap between lab and industry. Specifically, these challenges include effective heat dissipation, maintaining a high yield and having control of porosity of the product. Achieving fine control over the reaction and ensuring this control is not lost at larger scales should therefore be the high-level focus of future work. Multiple pathways to address these challenges were discussed in this perspective which we hope will provide a roadmap for future research directions in the p-Si synthesis field. By leveraging technological advancements and maintaining a system-level perspective, p-Si can play a pivotal role in the future of sustainable energy, contributing to a greener and more efficient energy landscape.

Data availability

All the data that support this study are included in this article and its ESI files.†

Author contributions

All authors contributed to the conceptualization and writing of the article. M. Y. and S. A. drafted the initial manuscript, S. P. provided input and revisions, and M. D. performed the final editing.

Conflicts of interest

There are no conflicts to declare.

Acknowledgements

MY and SP would like to thank the CDT for Energy Storage and its Applications (EP/L016818/1) for financial support. MY and SP would also like to thank the Faraday Institution (Seed Project FIRG041 and Industry Sprint Project FIRG068) for financial support. MD thanks the Natural Sciences and Engineering Research Council of Canada (NSERC) Discovery Grant and Killam Trusts for the research funding. SM thanks NSERC for a graduate fellowship and Mitacs for financial support. Matthew Margeson is thanked for assisting with the figures.

References

1 T. Ahmad and D. Zhang, A critical review of comparative global historical energy consumption and future demand: the story told so far, *Energy Rep.*, 2020, **6**, 1973–1991.
2 J. Entwistle, A. Rennie and S. Patwardhan, A review of magnesiothermic reduction of silica to porous silicon for lithium-ion battery applications and beyond, *J. Mater. Chem. A*, 2018, **6**, 18344–18356.
3 Z. Yang, Y. Du, G. Hou, Y. Ouyang, F. Ding and F. Yuan, Nanoporous silicon spheres preparation *via* a controllable magnesiothermic reduction as anode for Li-ion batteries, *Electrochim. Acta*, 2020, **329**, 135141.
4 J.-F. Wang, K.-X. Wang, F.-H. Du, X.-X. Guo, Y.-M. Jiang and J.-S. Chen, Amorphous silicon with high specific surface area

prepared by a sodiothermic reduction method for supercapacitors, *Chem. Commun.*, 2013, **49**, 5007–5009.

5 L. Wang, B. Gao, C. Peng, X. Peng, J. Fu, P. K. Chu and K. Huo, Bamboo leaf derived ultrafine Si nanoparticles and Si/C nanocomposites for high-performance Li-ion battery anodes, *Nanoscale*, 2015, **7**, 13840–13847.

6 L. Shi, W. Wang, A. Wang, K. Yuan and Y. Yang, Understanding the impact mechanism of the thermal effect on the porous silicon anode material preparation *via* magnesiothermic reduction, *J. Alloys Compd.*, 2016, **661**, 27–37.

7 J. Ryu, D. Hong, S. Choi and S. Park, Synthesis of Ultrathin Si Nanosheets from Natural Clays for Lithium-Ion Battery Anodes, *ACS Nano*, 2016, **10**, 2843–2851.

8 J. Ryu, S. Choi, T. Bok and S. Park, Nanotubular structured Si-based multicomponent anodes for high-performance lithium-ion batteries with controllable pore size *via* coaxial electro-spinning, *Nanoscale*, 2015, **7**, 6126–6135.

9 K. Mishra, J. Zheng, R. Patel, L. Estevez, H. Jia, L. Luo, P. Z. El-Khoury, X. Li, X.-D. Zhou and J.-G. Zhang, High performance porous Si@C anodes synthesized by low temperature aluminothermic reaction, *Electrochim. Acta*, 2018, **269**, 509–516.

10 N. Liu, K. Huo, M. T. McDowell, J. Zhao and Y. Cui, Rice husks as a sustainable source of nanostructured silicon for high performance Li-ion battery anodes, *Sci. Rep.*, 2013, **3**, 1–7.

11 N. Lin, Y. Han, J. Zhou, K. Zhang, T. Xu, Y. Zhu and Y. Qian, A low temperature molten salt process for aluminothermic reduction of silicon oxides to crystalline Si for Li-ion batteries, *Energy Environ. Sci.*, 2015, **8**, 3187–3191.

12 N. Kim, H. Park, N. Yoon and J. K. Lee, Zeolite-Templated Mesoporous Silicon Particles for Advanced Lithium-Ion Battery Anodes, *ACS Nano*, 2018, **12**, 3853–3864.

13 M. Furquan, A. Raj Khatribail, S. Vijayalakshmi and S. Mitra, Efficient conversion of sand to nano-silicon and its energetic Si-C composite anode design for high volumetric capacity lithium-ion battery, *J. Power Sources*, 2018, **382**, 56–68.

14 W. C. Cho, H. J. Kim, H. I. Lee, M. W. Seo, H. W. Ra, S. J. Yoon, T. Y. Mun, Y. K. Kim, J. H. Kim, B. H. Kim, J. W. Kook, C.-Y. Yoo, J. G. Lee and J. W. Choi, 5L-Scale Magnesio-Milling Reduction of Nanostructured SiO_2 for High Capacity Silicon Anodes in Lithium-Ion Batteries, *Nano Lett.*, 2016, **16**, 7261–7269.

15 H. Song, D. Liu, J. Yang, L. Wang, H. Xu and Y. Xiong, Highly Crystalline Mesoporous Silicon Spheres for Efficient Visible Photocatalytic Hydrogen Evolution, *ChemNanoMat*, 2017, **3**, 22–26.

16 J. Ryu, Y. J. Jang, S. Choi, H. J. Kang, H. Park, J. S. Lee and S. Park, All-in-one synthesis of mesoporous silicon nanosheets from natural clay and their applicability to hydrogen evolution, *NPG Asia Mater.*, 2016, **8**, e248.

17 S. A. Martell, U. Werner-Zwanziger and M. Dasog, The influence of hydrofluoric acid etching process on the photocatalytic hydrogen evolution reaction using mesoporous silicon nanoparticles, *Faraday Discuss.*, 2019, **222**, 176–189.

18 H. Sun, J. Chen, S. Liu, D. K. Agrawal, Y. Zhao, D. Wang and Z. Mao, Photocatalytic H_2 evolution of porous silicon derived from magnesiothermic reduction of mesoporous SiO_2, *Int. J. Hydrogen Energy*, 2019, **44**, 7216–7221.

19 F. Dai, J. Zai, R. Yi, M. L. Gordin, H. Sohn, S. Chen and D. Wang, Bottom-up synthesis of high surface area mesoporous crystalline silicon and evaluation of its hydrogen evolution performance, *Nat. Commun.*, 2014, **5**, 3605.

20 A. Islam, S. H. Teo, Md. R. Awual and Y. H. Taufiq-Yap, Assessment of clean H_2 energy production from water using novel silicon photocatalyst, *J. Cleaner Prod.*, 2020, **244**, 118805.

21 Z. Guo, L. J. Arachchige, S. Qiu, X. Zhang, Y. Xu, S. J. Langford and C. Sun, p-Block element-doped silicon nanowires for nitrogen reduction reaction: a DFT study, *Nanoscale*, 2021, **13**, 14935–14944.

22 K. Ithisuphalap, H. Zhang, L. Guo, Q. Yang, H. Yang and G. Wu, Photocatalysis and Photoelectrocatalysis Methods of Nitrogen Reduction for Sustainable Ammonia Synthesis, *Small Methods*, 2019, **3**, 1800352.

23 W. Sun, X. Yan, C. Qian, P. Nicholson Duchesne, S. G. H. Kumar and G. Ozin, The Next Big Thing for Silicon Nanostructures – CO_2 Photocatalysis, *Faraday Discuss.*, 2019, **222**, 424–432.

24 C. A. Betty, R. Sasikala, O. D. Jayakumar, T. Sakuntala and A. K. Tyagi, Photoelectrochemical properties of porous silicon based novel photoelectrodes, *Prog. Photovolt.: Res. Appl.*, 2011, **19**, 266–274.

25 S. Chandrasekaran, S. Vijayakumar, T. Nann and N. H. Voelcker, Investigation of porous silicon photocathodes for photoelectrochemical hydrogen production, *Int. J. Hydrogen Energy*, 2016, **41**, 19915–19920.

26 C. Sun, Z. Shao, Y. Hu, Y. Peng and Q. Xie, Photoelectrocatalysis Synthesis of Ammonia Based on a Ni-Doped MoS_2/Si Nanowires Photocathode and Porous Water with High N_2 Solubility, *ACS Appl. Mater. Interfaces*, 2023, **15**, 23085–23092.

27 I. Roh, S. Yu, C.-K. Lin, S. Louisia, S. Cestellos-Blanco and P. Yang, Photoelectrochemical CO_2 Reduction toward Multicarbon Products with Silicon Nanowire Photocathodes Interfaced with Copper Nanoparticles, *J. Am. Chem. Soc.*, 2022, **144**, 8002–8006.

28 S. A. Martell, Y. Lai, E. Traver, J. MacInnis, D. D. Richards, S. MacQuarrie and M. Dasog, High Surface Area Mesoporous Silicon Nanoparticles Prepared *via* Two-Step Magnesiothermic Reduction for Stoichiometric CO_2 to CH_3OH Conversion, *ACS Appl. Nano Mater.*, 2019, **2**, 5713–5719.

29 M. Dasog, S. Kraus, R. Sinelnikov, J. G. C. Veinot and B. Rieger, CO_2 to methanol conversion using hydride terminated porous silicon nanoparticles, *Chem. Commun.*, 2017, **53**, 3114–3117.

30 W. Sun, C. Qian, L. He, K. K. Ghuman, A. P. Y. Wong, J. Jia, A. A. Jelle, P. G. O'Brien, L. M. Reyes, T. E. Wood, A. S. Helmy, C. A. Mims, C. V. Singh and G. A. Ozin, Heterogeneous

reduction of carbon dioxide by hydride-terminated silicon nanocrystals, *Nat. Commun.*, 2016, **7**, 12553.
31 M. Dasog, G. B. De los Reyes, L. V. Titova, F. A. Hegmann and J. G. C. Veinot, Size *vs.* Surface: Tuning the Photoluminescence of Freestanding Silicon Nanocrystals Across the Visible Spectrum *via* Surface Groups, *ACS Nano*, 2014, **8**, 9636–9648.
32 S. Alexandrou and J. P. Cook, Silicon fuel: a hydrogen storage material, *Int. J. Hydrogen Energy*, 2021, **46**, 1627–1633.
33 F. Erogbogbo, T. Lin, P. M. Tucciarone, K. M. LaJoie, L. Lai, G. D. Patki, P. N. Prasad and M. T. Swihart, On-Demand Hydrogen Generation using Nanosilicon: Splitting Water without Light, Heat, or Electricity, *Nano Lett.*, 2013, **13**, 451–456.
34 J. E. Entwistle, G. Beaucage and S. V. Patwardhan, Mechanistic understanding of pore evolution enables high performance mesoporous silicon production for lithium-ion batteries, *J. Mater. Chem. A*, 2020, **8**, 4938–4949.
35 A. Franco Gonzalez, N.-H. Yang and R.-S. Liu, Silicon Anode Design for Lithium-Ion Batteries: Progress and Perspectives, *J. Phys. Chem. C*, 2017, **121**, 27775–27787.
36 I. S. Curtis, R. J. Wills and M. Dasog, Photocatalytic hydrogen generation using mesoporous silicon nanoparticles: influence of magnesiothermic reduction conditions and nanoparticle aging on the catalytic activity, *Nanoscale*, 2021, **13**, 2685–2692.
37 S. Chandrasekaran, T. Nann and N. H. Voelcker, Nanostructured silicon photoelectrodes for solar water electrolysis, *Nano Energy*, 2015, **17**, 308–322.
38 T. Mizutani, H. Ohta, T. Ueda, T. Kashiwagi, T. Fukuda, T. Shiobara and K. Saitow, Mechanochemically Tailored Silicon Particles for Efficient H_2 Production: Entropy and Enthalpy Engineering, *ACS Sustain. Chem. Eng.*, 2023, **11**, 11769–11780.
39 X. H. Liu, L. Zhong, S. Huang, S. X. Mao, T. Zhu and J. Y. Huang, Size-Dependent Fracture of Silicon Nanoparticles During Lithiation, *ACS Nano*, 2012, **6**, 1522–1531.
40 L. Canham, in *Handbook of Porous Silicon*, ed. L. Canham, Springer International Publishing, Cham, 2014, pp. 3–9.
41 W. Simmler, in *Ullmann's Encyclopedia of Industrial Chemistry*, Wiley VCH, Weinheim, Germany, 7th edn, 2011, pp. 1–29.
42 S. G. Hutchison, L. S. Richardson and C. M. Wai, Carbothermic reduction of silicon dioxide—a thermodynamic investigation, *Metall. Trans. B*, 1988, **19**, 249–253.
43 L. Armando, in *Handbook of mpSi*, Springer, Malvern, UK, 2014, pp. 11–22.
44 J. Jakubowicz, in *Handbook of Porous Silicon*, Springer International Publishing, 2014, pp. 93–102.
45 W. Simmler, in *Ullmann's Encyclopedia of Industrial Chemistry*, Wiley VCH, Weinheim, Germany, 7th edn, 2011, pp. 1–17.
46 S. J. P. McInnes, E. J. Szili, S. A. Al-Bataineh, R. B. Vasani, J. Xu, M. E. Alf, K. K. Gleason, R. D. Short and N. H. Voelcker, Fabrication and Characterization of a Porous Silicon Drug Delivery System with an Initiated Chemical Vapor Deposition Temperature-Responsive Coating, *Langmuir*, 2016, **32**, 301–308.
47 V. S. Ban and S. L. Gilbert, The chemistry and transport phenomena of chemical vapor deposition of silicon from $SiCl_4$, *J. Cryst. Growth*, 1975, **31**, 284–289.
48 N. Harpak, G. Davidi, D. Schneier, S. Menkin, E. Mados, D. Golodnitsky, E. Peled and F. Patolsky, Large-Scale Self-Catalyzed Spongelike Silicon Nano-Network-Based 3D Anodes for High-Capacity Lithium-Ion Batteries, *Nano Lett.*, 2019, **19**, 1944–1954.
49 M. Nagamori, I. Malinsky and A. Claveau, Thermodynamics of the Si-C-O system for the production of silicon carbide and metallic silicon, *Metall. Trans. B*, 1986, **17**, 503–514.
50 M. Hasegawa, in *Treatise on Process Metallurgy*, ed. S. Seetharaman, Elsevier, Boston, 2014, pp. 507–516.
51 C. B. Alcock, V. P. Itkin and M. K. Horrigan, Vapour Pressure Equations for the Metallic Elements: 298–2500 K, *Can. Metall. Q.*, 1984, **23**, 309–313.
52 A. Fedoročková and P. Raschman, Effects of pH and acid anions on the dissolution kinetics of MgO, *Chem. Eng. J.*, 2008, **143**, 265–272.
53 P. Mishra, A. Chakraverty and H. D. Banerjee, Production and purification of silicon by calcium reduction of rice-husk white ash, *J. Mater. Sci.*, 1985, **20**, 4387–4391.
54 J.-F. Wang, J.-S. Chen and Z.-F. Zhou, Preparation of Porous Silicon by Sodiothermic Reduction of Zeolite and Photoactivation for Benzene Oxidation, *Eur. J. Inorg. Chem.*, 2015, **2015**, 1330–1333.
55 Y. Lai, J. R. Thompson and M. Dasog, Metallothermic Reduction of Silica Nanoparticles to Porous Silicon for Drug Delivery Using New and Existing Reductants, *Chem.–Eur. J.*, 2018, **24**, 7913–7920.
56 K. Yasuda and T. H. Okabe, Solar-grade silicon production by metallothermic reduction, *JOM*, 2010, **62**, 94–101.
57 J. D. Lee, in *Concise Inorganic Chemistry*, Chapman & Hall, 5th edn, 1996, p. 976.
58 H. D. Banerjee, S. Sen and H. N. Acharya, Investigations on the production of silicon from rice husks by the magnesium method, *Mater. Sci. Eng.*, 1982, **52**, 173–179.
59 Z. Bao, M. R. Weatherspoon, S. Shian, Y. Cai, P. D. Graham, S. M. Allan, G. Ahmad, M. B. Dickerson, B. C. Church, Z. Kang, H. W. A. Iii, C. J. Summers, M. Liu and K. H. Sandhage, Chemical reduction of three-dimensional silica micro-assemblies into microporous silicon replicas, *Nature*, 2007, **446**, 172–175.
60 B. Zhang, F. Wang, J. Chen, B. Li, K. Liu and Q. Han, A Study on the Heat Effect during Magnesiothermic Reduction of Porous SiO_2, *Silicon*, 2022, **14**, 8409–8416.
61 I. Gutman, I. Gotman and M. Shapiro, Kinetics and mechanism of periodic structure formation at SiO_2/Mg interface, *Acta Mater.*, 2006, **54**, 4677–4684.
62 J. Liang, X. Li, Z. Hou, W. Zhang, Y. Zhu and Y. Qian, A Deep Reduction and Partial Oxidation Strategy for Fabrication of Mesoporous Si Anode for Lithium Ion Batteries, *ACS Nano*, 2016, **10**, 2295–2304.

63 J.-K. Yoo, J. Kim, M.-J. Choi, Y.-U. Park, J. Hong, K. M. Baek, K. Kang and Y. S. Jung, Extremely High Yield Conversion from Low-Cost Sand to High-Capacity Si Electrodes for Li-Ion Batteries, *Adv. Energy Mater.*, 2014, **4**, 1400622.

64 K. C. Nandi, D. Mukherjee, A. K. Biswas and H. N. Acharya, Optimization of acid concentration, temperature and particle size of magnesium silicide, obtained from rice husk, for the production of silanes, *J. Mater. Sci. Lett.*, 1993, **12**, 1248–1250.

65 K. Kamitsuji, T. Sato, H. Suzuki and C. Kaito, Direct observation of crystallization of amorphous Mg-bearing silicate grains into Mg (forsterite), *Astron. Astrophys.*, 2005, **436**, 165–169.

66 G. W. Brindley and R. Hayami, Kinetics and mechanism of formation of forsterite (Mg_2SiO_4) by solid state reaction of MgO and SiO_2, *Philos. Mag.*, 1965, **12**, 505–514.

67 Y. Tan, T. Jiang and G. Z. Chen, Mechanisms and Product Options of Magnesiothermic Reduction of Silica to Silicon for Lithium-Ion Battery Applications, *Front. Energy Res.*, 2021, **9**, 98.

68 A. Rasouli, K. E. Herstad, J. Safarian and G. Tranell, Magnesiothermic Reduction of Natural Quartz, *Metall. Mater. Trans. B*, 2022, **53**, 2132–2142.

69 S. Martell, M. Yan, R. Coridan, K. Stone, S. Patwardhan and M. Dasog, Unlocking the secrets of porous silicon formation: insights into magnesiothermic reduction mechanism using in situ powder X-ray diffraction studies, *Nanoscale Horiz.*, 2024, DOI: **10.1039/D4NH00244J**.

70 M. Yan, S. Martell, M. Dasog, S. Brown and S. V. Patwardhan, Cost-competitive manufacture of porous-silicon anodes *via* the magnesiothermic reduction: a techno-economic analysis, *J. Power Sources*, 2023, **588**, 233720.

71 M. Yan and S. V. Patwardhan, Exploiting nanoscale effects enables ultra-low temperature to produce porous silicon, *RSC Adv.*, 2021, **11**, 35182–35186.

72 M. Auffan, J. Rose, M. R. Wiesner and J.-Y. Bottero, Chemical stability of metallic nanoparticles: a parameter controlling their potential cellular toxicity in vitro, *Environ. Pollut.*, 2009, **157**, 1127–1133.

73 L. Xu, H.-W. Liang, Y. Yang and S.-H. Yu, Stability and Reactivity: Positive and Negative Aspects for Nanoparticle Processing, *Chem. Rev.*, 2018, **118**, 3209–3250.

74 G. D. Stucky, X. Hu, Y. Zhao, H. Wang and N. Maru, Multi-Stage Magnesiothermic Reduction for Production of Silicon Oxides with Reduced Silicon Grain Size, *US Pat.*, US20230108286A1, April 6, 2023.

75 Z. Fan, W.-R. Liu, L. Sun, A. Nishio, R. Szczęsny, Y.-G. Lin, S. Okada and D. H. Gregory, Carbon-Free Conversion of SiO_2 to Si *via* Ultra-Rapid Alloy Formation: Toward the Sustainable Fabrication of Nanoporous Si for Lithium-Ion Batteries, *ACS Appl. Mater. Interfaces*, 2023, **15**, 36076–36085.

76 X. Yang, C. Zhan, D. Xu, D. Nan, R. Lv, W. Shen, F. Kang and Z.-H. Huang, SiO_x@Si-graphite microspheres for high-stable anode of lithium-ion batteries, *Electrochim. Acta*, 2022, **426**, 140795.

77 J. Zhang, Z. Hou, X. Zhang, L. Zhang and C. Li, Delicate construction of Si@SiO_x composite materials by microwave hydrothermal for lithium-ion battery anodes, *Ionics*, 2020, **26**, 69–74.

78 S. Haouli, S. Boudebane, I. J. Slipper, S. Lemboub, P. Gebara and S. Mezrag, Combustion synthesis of silicon by magnesiothermic reduction, *Phosphorus, Sulfur Silicon Relat. Elem.*, 2018, **193**, 280–287.

79 S. Putwa, I. S. Curtis and M. Dasog, Nanostructured silicon photocatalysts for solar-driven fuel production, *iScience*, 2023, **26**, 106317.

80 H. Kim, M. Seo, M.-H. Park and J. Cho, A Critical Size of Silicon Nano-Anodes for Lithium Rechargeable Batteries, *Angew. Chem., Int. Ed.*, 2010, **49**, 2146–2149.

81 M. J. Kirshenbaum, M. G. Boebinger, M. J. Katz, M. T. McDowell and M. Dasog, Solid-State Route for the Synthesis of Scalable, Luminescent Silicon and Germanium Nanocrystals, *ChemNanoMat*, 2018, **4**, 423–429.

82 J. Xie, G. Wang, Y. Huo, S. Zhang, G. Cao and X. Zhao, Nanostructured silicon spheres prepared by a controllable magnesiothermic reduction as anode for lithium ion batteries, *Electrochim. Acta*, 2014, **135**, 94–100.

83 M. Mezbahul-Islam, A. O. Mostafa and M. Medraj, Essential Magnesium Alloys Binary Phase Diagrams and Their Thermochemical Data, *J. Mater.*, 2014, **1**, 704283.

84 L. Khanna, Y. Lai and M. Dasog, Systematic evaluation of inorganic salts as a heat sink for the magnesiothermic reduction of silica, *Can. J. Chem.*, 2018, **96**, 965–968.

85 X. Chen, S. Wei, Y. Yan, F. Tong, G. I. N. Waterhouse, T. Söhnel, M. P. Taylor and P. Cao, Dissolution Mechanism of Eutectic and Hypereutectic Mg–Sn Alloy Anodes for Magnesium Rechargeable Batteries, *ACS Appl. Mater. Interfaces*, 2023, **15**, 33065–33076.

86 R. N. Abdullaev, D. A. Samoshkin, A. Sh. Agazhanov and S. V. Stankus, Heat Capacity of Pure Magnesium and Ultralight Congruent Magnesium–Lithium Alloy in the Temperature Range of 300 K to 825 K, *J. Eng. Thermophys.*, 2021, **30**, 207–212.

87 R. Pilling, S. R. Coles, M. R. Knecht and S. V. Patwardhan, Multi-criteria discovery, design and manufacturing to realise nanomaterial potential, *Communications Engineering*, 2023, **2**, 1–6.

88 A. M. Schweidtmann, E. Esche, A. Fischer, M. Kloft, J.-U. Repke, S. Sager and A. Mitsos, Machine Learning in Chemical Engineering: A Perspective, *Chem. Ing. Tech.*, 2021, **93**, 2029–2039.

89 K. Tang, A. Rasouli, J. Safarian, X. Ma and G. Tranell, Magnesiothermic Reduction of Silica: A Machine Learning Study, *Materials*, 2023, **16**, 4098.

90 Andriayani, S. Lumban Raja, A. Hamzah Siregar, A. Daulay and S. Sudarman, Synthesis of silicon nanoparticles with various additions of inert salt as scavenger agent during reduction by the magnesiothermic method as anode lithium-ion batteries, *Mater. Sci. Energy Technol.*, 2024, **7**, 148–157.

91 N. Yoon, C. Young, D. Kang, H. Park and J. K. Lee, High-conversion reduction synthesis of porous silicon for advanced lithium battery anodes, *Electrochim. Acta*, 2021, **391**, 138967.